Mixing performance in continuous oscillatory baffled reactors

Marco Antonio Ávila López, David F. Fletcher, Martine Poux, Catherine Xuereb, Joelle Aubin

▶ **To cite this version:**

Marco Antonio Ávila López, David F. Fletcher, Martine Poux, Catherine Xuereb, Joelle Aubin. Mixing performance in continuous oscillatory baffled reactors. Chemical Engineering Science, 2020, 219, pp.115600. ⟨10.1016/j.ces.2020.115600⟩. ⟨hal-02735360⟩

HAL Id: hal-02735360

https://hal.science/hal-02735360v1

Submitted on 2 Jun 2020

HAL is a multi-disciplinary open access archive for the deposit and dissemination of scientific research documents, whether they are published or not. The documents may come from teaching and research institutions in France or abroad, or from public or private research centers.

L'archive ouverte pluridisciplinaire **HAL**, est destinée au dépôt et à la diffusion de documents scientifiques de niveau recherche, publiés ou non, émanant des établissements d'enseignement et de recherche français ou étrangers, des laboratoires publics ou privés.

HAL Authorization

OATAO

Open Archive Toulouse Archive Ouverte

Open Archive Toulouse Archive Ouverte

OATAO is an open access repository that collects the work of Toulouse researchers and makes it freely available over the web where possible

This is an author's version published in: http://oatao.univ-toulouse.fr/25846

Official URL:

https://doi.org/10.1016/j.ces.2020.115600

To cite this version:

Ávila López, Marco Antonio and Fletcher, David F. and Poux, Martine and Xuereb, Catherine and Aubin, Joelle *Mixing performance in continuous oscillatory baffled reactors.* (2020) Chemical Engineering Science, 219. 115600. ISSN 0009-2509.

Any correspondence concerning this service should be sent to the repository administrator: tech-oatao@listes-diff.inp-toulouse.fr

Mixing performance in continuous oscillatory baffled reactors

M. Avila [a], D.F. Fletcher [b], M. Poux [a], C. Xuereb [a], J. Aubin [a,*]

[a] Laboratoire de Génie Chimique, Université de Toulouse, CNRS, INPT, UPS, Toulouse, France
[b] School of Chemical and Biomolecular Engineering, The University of Sydney, NSW 2006, Australia

GRAPHICAL ABSTRACT

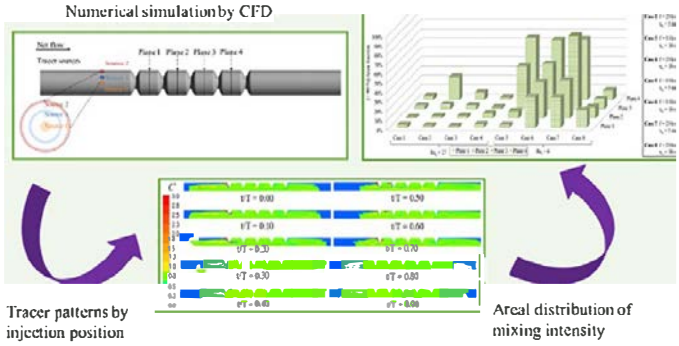

ABSTRACT

In the current literature, there is limited information on the influence of operating parameters on spatial mixing quality and how a secondary feed should be introduced into continuous oscillatory baffled reactors (COBR) to achieve good mixing quality. This work explores for the first time the impact of the position of a secondary feed (passive non reactive tracer) on spatial mixing performance in a COBR using transient laminar CFD simulations. Three theoretical feed positions are studied covering a range of net flow and oscillatory Reynolds numbers ($Re_{net} = 6$ 27/$Re_o = 24$ 96), the range being chosen to ensure that the flow field remains two dimensional in all cases. Macromixing is evaluated by analysing the spatial uniformity of the tracer with the areal distribution method developed by Alberini et al. (2014a). Introduction of the secondary stream at the reactor wall or upstream of the edge of the first baffle greatly improves mixing quality due to the recirculation eddies, which assist radial mixing. However, introduction of the secondary feed at the centreline results in high axial dispersion with limited radial mixing. With an adequate introduction position, mixing quality typically increases with an increment in the velocity ratio. Nevertheless, if the net flow is too low, mixing performance decreases because the secondary stream is pushed upstream of the baffles, where it does not benefit from flow recirculation.

Keywords:
CFD
Continuous oscillatory flow
COBR
Macromixing
Laminar flow

1. Introduction

Due to the combination of net flow and pulsations, as well as the interaction of this flow with baffles, continuous oscillatory baffled reactors (COBRs) offer interesting advantages over traditional mixing processes in stirred tanks and provide a means for process intensification. A schematic diagram of a COBR, composed of a tube

* Corresponding author at: Laboratoire de Génie Chimique, 4 allée Emile Monso BP-84234, 31432 Toulouse Cedex 4, France.
E-mail address: joelle.aubin@ensiacet.fr (J. Aubin).

Nomenclature

C^*	dimensionless tracer concentration ( )
C_i^*	local dimensionless tracer concentration at the time t ( )
C_i	local scalar concentration of the tracer at time t (kg m ^{3})
C_0	concentration of tracer in the injection source (kg m ^{3})
$\bar{C}$	fully mixed concentration (kg m ^{3})
C_X	lower limit of mixedness range ( )
C_{X_+}	upper limit of mixedness range ( )
D	COBR diameter (m)
D_f	diffusion coefficient (m^2 s ^{1})
f	oscillation frequency (Hz)
l_b	distance between baffles (m)
p	pressure (Pa)
q	volumetric flow rate at the tracer inlet (m^3 s ^{1})
Q	volumetric flow rate at the COBR inlet (m^3 s ^{1})
R	radius of reactor (m)
Re_{net}	net flow Reynold number ( )
Re_o	oscillatory Reynolds number ( )
r	radial coordinate (m)
r_n	radial number ( )
Sc	Schmidt number ( )
$\dot{S}_C$	mass source of tracer (kg m ^{3} s ^{1})
S_n	swirl number ( )
St	Strouhal number ( )
t	time (s)
T	oscillation period (s)
u_{in}	initial velocity (m s ^{1})
$\underline{u}$	instantaneous velocity (m s ^{1})
$\bar{u}$	mean velocity (m s ^{1})
u_{net}	net velocity (m s ^{1})
u_{max}	maximal velocity ($u_{net} + 2\pi x_o$) (m s ^{1})
v_r	radial velocity (m s ^{1})
v_z	axial velocity (cylindrical coordinate) (m s ^{1})
v_θ	tangential velocity (m s ^{1})
u_x	axial velocity (cartesian coordinate) (m s ^{1})
$\boldsymbol{u}$	velocity vector (m s ^{1})
x_o	oscillation amplitude (m)
x, y, z	cartesian coordinates (m)
X	percentage of perfectly mixed state ( )

Greek symbols

μ	dynamic viscosity (Pa s)
ρ	fluid density (kg m ^{3})
τ	shear stress tensor (Pa)
ψ	velocity ratio ( )

with single orifice plate baffles, is shown in Fig. 1. The interaction of the pulsed flow with baffles creates complex hydrodynamics with recirculating eddies in COBRs, resulting in effective mixing, mass and heat transfer, as well as plug flow in both laminar and transitional flow regimes (Mackley and Stonestreet, 1995; Ni et al., 2000; Stephens and Mackley, 2002) and in compact geome tries (i.e. reduced length to diameter ratio tube) (Harvey et al., 2001).

Continuous oscillatory flow in COBRs is characterized by differ ent dimensionless numbers, such as the net flow Reynolds number (Re_{net}), oscillatory Reynolds number (Re_o), Strouhal number (St), and velocity ratio (ψ), which are defined as:

$$Re_{net} \quad \frac{\rho u_{net} D}{\mu} \tag{1}$$

$$Re_o \quad \frac{2\pi \rho f x_o D}{\mu} \tag{2}$$

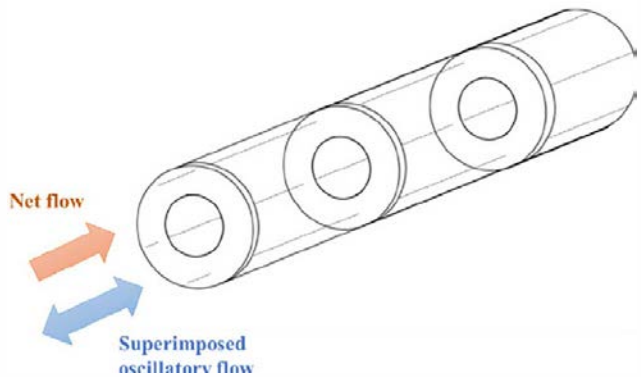

Fig. 1. Schematic diagram of a continuous oscillatory baffled reactor with a standard single orifice plate geometry.

$$St \quad \frac{D}{4\pi x_o} \tag{3}$$

$$\psi \quad \frac{Re_o}{Re_{net}} \tag{4}$$

where ρ is the fluid density, u_{net} is the net velocity magnitude, D is the pipe diameter, μ is the dynamic viscosity, f is the frequency of oscillation, and x_o is the oscillation amplitude.

InRe_o, the characteristic velocity is the maximum oscillatory velocity. Re_o has been used to describe the intensity of mixing in the COBR and Stonestreet and Van Der Veeken (1999) identified different flow regimes. For $Re_o < 250$, the flow is essentially 2 dimensional and axi symmetric with low mixing intensity; for $Re_o > 250$, the flow becomes 3 dimensional and mixing is more intense; finally, when $Re_o > 2000$, the flow is fully turbulent. The Strouhal number measures the effective eddy propagation with relation to the tube diameter. Higher values of St induce the prop agation of the eddies into the next baffle zone (Ahmed et al., 2017). The most common range of the Strouhal number used in the liter ature is $0.15 < St < 4$ (Abbott et al., 2013). The velocity ratio, ψ, describes the relationship between the oscillatory and net flow. It is typically recommended to operate at a velocity ratio greater than 1 to ensure that the oscillatory flow dominates the superimposed net flow (Stonestreet and Van Der Veeken, 1999). This ratio has been used largely to describe the plug flow behaviour in the COBR.

Amongst the different works that study mixing in COBRs, most have focused on flow patterns, velocity profiles, plug behaviour (Dickens et al., 1989; Hewgill et al., 1993; Kacker et al., 2017; Mackley and Ni, 1993; Manninen et al., 2013; Ni, 1995; Phan and Harvey, 2010, 2011), or the conversion rate of chemical reactions (Eze et al., 2017; Harvey et al., 2003; Lobry et al., 2014; Mazubert et al., 2015; Phan et al., 2012; Soufi et al., 2017). These velocity profiles and flow patterns, which have been determined by Particle Image Velocimetry (PIV) or Computational Fluids Dynamics (CFD) (Amokrane et al., 2014; González Juárez et al., 2017; Mazubert et al., 2016a; McDonough et al., 2017;

Ni et al., 2003), are used to understand how the geometrical parameters and dimensionless groups affect the hydrodynamics of the continuous oscillatory flow.

Concerning the characterisation of mixing quality, the main objectives of the previous work presented in the literature are to evaluate the plug flow behaviour via the residence time distribution (RTD) and to determine the operating conditions required to achieve the narrowest RTD (Abbott et al., 2014; Dickens et al., 1989; Kacker et al., 2017; Mackley and Ni, 1991; Reis et al., 2004). Most of these studies are experimental and have analysed the dispersion of a pulse injection of homogeneous tracer in the continuous phase as a function of the oscillatory and net flow conditions, as well as the geometrical parameters of the COBR. From these studies, the recommended range of the oscillatory to net velocity ratio, ψ, to ensure plug flow operation (such that radial flow dominates and limits axial dispersion) is between 2 and 4 (Stonestreet and Van Der Veeken, 1999). However, these recommendations are not always used in practice. For example, many continuous crystallization processes in oscillatory baffled reactors have been operated with velocity ratios near the upper limit of the recommended range, or even with higher values, to ensure solid suspension and uniform particle size and distribution (Briggs et al., 2015; Kacker et al., 2017; Peña et al., 2017; Siddique et al., 2015; Zhao et al., 2014). Indeed, whilst RTD measurements are a good means to characterize mixing in COBRs for operations that require long residence times (e.g. crystallisation and polymerisation), plug flow and RTD may not necessarily be the only characteristics that should be taken into consideration when operating conditions are chosen for this type of reactor. Indeed, depending on the process objective, other characteristics may be important for quantifying mixing, such as the spatial homogeneity of a minor species or a second phase (e.g. solid suspension), or even micromixing and how fast the fluids are mixed (Kukukova et al., 2009).

Very few studies have addressed mixing performance in COBRs in other ways than evaluating RTD. Ni et al. (1998) characterized oscillatory baffled columns using the time necessary for a tracer to reach a specific uniform concentration into the column. Mazubert et al., 2016a, 2016b developed methods to evaluate radial and axial fluid stretching and shear strain rate history in the COBR. The first method allows spatial mixing to be assessed and to identify the presence of chaotic flow; the second technique is useful for operations that are shear dependent, e.g. droplet break up. McDonough et al. (2017) characterized mixing in a COBR with helical baffles using PIV and numerical simulation. They used the swirl and radial numbers to identify whether mixing is dominated by swirl or vortex flows. The swirl number describes the ratio of the axial flux of angular momentum to the axial flux of linear momentum:

$$S_n \quad \frac{\int_Z^v v_z v_\theta r^2 \mathrm{d}r}{R \int v_z^2 r \mathrm{d}r} \tag{5}$$

where v_z and v_θ are the axial and tangential velocity components, r is the radial position, and R the hydraulic radius. The radial number compares the axial flux of radial momentum to the axial flux of axial momentum:

$$r_n \quad \frac{\int_Z^v v_z v_r r \mathrm{d}r}{\int v_z^2 r \mathrm{d}r} \tag{6}$$

In a more recent study, McDonough et al. (2019) characterized micromixing in different meso COBR geometries with the Villermaux Dushman test reaction, which is of interest for fast reactions or operations with fast kinetics such as precipitations.

Considering the current information on mixing in COBRs available in the literature, there is little knowledge on the effect of operating parameters on spatial mixing quality and how a secondary feed should be injected into the COBR to achieve good mixing performance. Indeed, improved mixing performance would typically lead to enhanced process performance, however it could also lead to more compact reactor designs and provide opportunities for new applications (other than reactions with slow kinetics), e.g. precipitation/crystallization processes that require long residence times to allow particle or crystal growth, but also fast mixing in the first stage of the reactor.

Determination of spatial mixing quality in COBRs requires knowledge of concentration fields of a tracer in cross sections along the length of the reactor. Whilst information of this type can be obtained experimentally using Planar Laser Induced Fluorescence (PLIF), its application to COBRs (in which mixing relies on the interaction of oscillatory flow with the reactor baffles upstream of the measurement plane) is technically not feasible. CFD simulations are therefore an attractive solution to evaluate three dimensional spatial mixing quality in COBRs. Nevertheless, such simulations are not without major challenges, including the need for a highly refined mesh on a sufficiently long reactor model and the consequent computational resources in order to correctly resolve the time dependent concentration gradients.

The objective of this study is to begin to explore the impact of the position where a secondary feed enters the COBR on the spatial mixing quality. To do this, transient laminar flow CFD simulations are performed for a passive non reactive tracer, which is released in the COBR in three theoretical ways in a NiTech® COBR with smooth constrictions. The simulations enable access to time resolved concentration fields throughout the volume of the reactor and the influence of operating conditions on macromixing performance is evaluated by analysing the spatial uniformity of the tracer using the areal distribution method developed by Alberini et al. (2014a).

2. Characterization of mixing performance

2.1. Statistical analysis of concentration distribution

Mixing performance was evaluated by studying the tracer concentration over the reactor length. The uniformity of tracer concentration is assessed at different cross sections in the COBR, each located midway between baffles. The dimensionless tracer concentration in each computational cell, C_i^*, is:

$$C_i^* \quad \frac{C_i}{C} \tag{7}$$

where $C_i$is the instantaneous tracer concentration and C corresponds to the fully mixed concentration assuming perfect blending of the tracer:

$$C \quad C_0\left(\frac{q}{Q+q}\right) \tag{8}$$

where C_0 is the concentration of tracer in the injected fluid, q is the mass flow of tracer and Q is the net flow rate.

The plane averaged concentration, C^*, of the non reactive tracer over cross sections at each time step of the transient solution and different times of the oscillatory cycle, t/T, was then calculated. If $C^* > C$, it is referred to in this study as overly concentrated.

2.2. Areal distribution of mixing intensity

The areal distribution method enables mixing intensity in laminar flow to be analysed by considering areas in a cross section that have the same level of mixing (Alberini et al., 2014a). The results of

the areal distribution of mixing intensity represent a record of how tracer is mixed over time, taking into account both the intensity of segregation (or uniformity of concentration) and the scale of segregation. This methodology enables identification of poorly mixed areas (both over concentrated and under concentrated regions), unlike the coefficient of variance or maximum striation thickness, which can lead to misleading interpretation of mixing performance when used separately (Alberini et al., 2014a; Kukukova et al., 2009, 2011).

In practice, the areal distribution method analyses the distribution of concentration at different cross sections in the flow that have been obtained by either experimental (e.g. PLIF) or numerical techniques. Based on the perfectly mixed concentration criterion C, the limits for a certain level of mixing, X%, can be defined. For example, to determine the amount of the cross sectional area that is in a state of 90% mixing or greater, two limits are firstly defined: $C_{X-} = 0.9C$ and $C_{X+} = 1.1C$. The total area whereby the concentration satisfies $C_{X-} < C_i < C_{X+}$ is then determined and this corresponds to the amount of fluid in the cross section, which is 90% mixed or greater.

3. Numerical method

3.1. Geometry and operating conditions

The geometry studied is the NiTech® COBR, which is a single orifice baffled reactor with smooth constrictions, as shown in Fig. 2(a). The COBR tube has a diameter of 15 mm with 7.5 mm diameter orifices; the distance between orifices (or inter baffle spacing), l_b, is 16.9 mm. The model test section comprises a tube of length 144.5 mm and five orifices. A smooth reduction at the orifices is modelled to best represent the real geometry of the NiTech® glass COBR, as shown in Fig. 2(b).

The fluid considered in these simulations is a single phase fluid with density $\rho = 997$ kg/m^3 and dynamic viscosity $\mu = 2 \times 10^{-2}$ Pa.s. Isothermal conditions are assumed. A Schmidt number (Sc) of 1000 is chosen, as this is characteristic of miscible liquid liquid systems.

A 2^k factorial design is chosen to study the interaction between oscillatory conditions (frequency and amplitude) and net flow, and their influence on the mixing performance. Two different levels are studied for each of the three variables and Table 1 lists the conditions used. The oscillatory frequency is set at either 1 Hz or 2 Hz and the oscillatory amplitude is either 5 mm or 10 mm, which corresponds to 30% and 60% of the baffle spacing. These values of amplitude fall in the optimal operational range of amplitudes described in previous studies (Brunold et al., 1989; Gough et al., 1997; Soufi et al., 2017). The net flow and oscillatory Reynolds numbers corresponding to these conditions are in the ranges 6.27 and 24.96, respectively, ensuring axi symmetrical laminar flow since it is well below the chaotic flow transition, i.e. for oscillatory Reynolds numbers less than 250 (Stonestreet and Van Der Veeken, 1999; Zheng et al., 2007). These flow conditions enable the COBR to be modelled in 2D, allowing computational times to be reduced drastically. To obtain a wider vision of the influence of operating conditions on mixing quality in the first sections of the reactor, the simulations cover values of the velocity ratio ψ outside the range for plug flow as recommended by Stonestreet and Van Der Veeken (1999).

In order to analyse mixing performance, a passive inert tracer is introduced into the reactor. The presence of this tracer has a minimal effect on the hydrodynamic flow of the fluid since the flow rate ratio $\left(\frac{q}{Q+q}\right)$ is set to 3×10^{-4}. It should be noted that the final results do not depend on this value since the concentration data are presented relative to the well mixed state. The tracer is introduced continuously at three different theoretical locations in the COBR. Source 0 is located at the centreline of the COBR, Source 1 is upstream of the edge of the first baffle, and Source 2 is at the wall of the reactor. Source 0 represents a coaxial source, and Sources 1 and 2 are annular sources, as shown in Fig. 2(b). Whilst the latter two are not practical possibilities for feed streams, the differences in the three locations enable the impact of the inlet location on

(a)

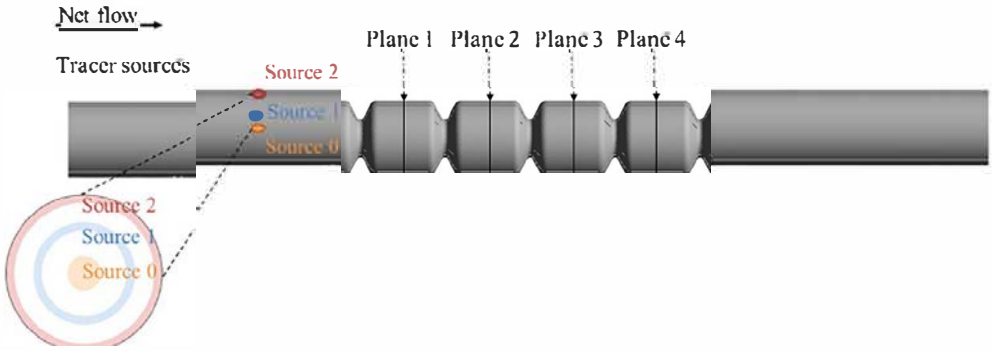

(b)

Fig. 2. (a) Photograph of the NiTech® COBR and (b) the geometry of the COBR simulated by CFD with the location of tracer sources and monitoring planes.

Table 1
Experimental conditions proposed by 2^k factorial design.

Case	Q(l h ^{1})	f(Hz)	x_o(mm)	Re_{net}	Re_o	Ψ
1	22.8	1	5	27	24	0.9
2	22.8	2	5	27	48	1.8
3	22.8	1	10	27	48	1.8
4	22.8	2	10	27	96	3.6
5	5.1	1	5	6	24	4.0
6	5.1	1	10	6	48	8.0
7	5.1	2	5	6	48	8.0
8	5.1	2	10	6	96	16.0

mixing to be evaluated. Due to the oscillatory flow, the tracer can flow out of the inlet and outlet boundaries. However, when the flow re enters the reactor it does not contain any tracer. This can result in erroneous concentration fields. Therefore, in order to guarantee that tracer is not lost via the inlet boundary condition, and that any the tracer that leaves and returns as new fluid (with out tracer) via the outlet does not reach the baffled zone, 30 mm portions of straight pipe have been added before and after the baf fled zone. Tracer concentration and mixing performance are anal ysed as described in Section 2 on four cross sectional planes located between the baffles, which are depicted in Fig. 2(b).

The numerical simulations of the flow in the COBR have been performed using the commercial package ANSYS Fluent 2019R3, which applies a finite volume discretization to solve the Navier Stokes equations.

For incompressible, laminar, Newtonian flow, the transient Navier Stokes equations for mass and momentum conservation are:

$$\nabla \cdot \boldsymbol{u} \quad \sum_{i\ 1}^{3} \dot{S}_{Ci} \tag{9}$$

$$\frac{\partial(\rho \boldsymbol{u})}{\partial t} + \nabla \cdot (\rho \boldsymbol{u} \otimes \boldsymbol{u}) \qquad \nabla p + \nabla \cdot \tau \tag{10}$$

The boundary condition at the inlet of the COBR is described by a time dependent velocity profile:

$$u_{in} \quad 2\,u \left(1 \quad \left(\frac{r}{R}\right)^2\right) \tag{11}$$

where r is the radial position R is the radius of the reactor and the mean velocity, u, is the sum of the velocity of the net flow and the oscillatory flow given by:

$$u \quad u_{net} + 2\pi f x_0 \sin(2\pi f t). \tag{12}$$

The gauge pressure was set to zero at the outlet and the tube wall was set to have no slip.

The transport of the tracer is described by the scalar transport equation without chemical reaction for incompressible flow:

$$\frac{\partial C_i}{\partial t} + \nabla \cdot (C_i \boldsymbol{u}) \quad \nabla \cdot \left(D_f \nabla C_i\right) \quad \dot{S}_{Ci} \tag{13}$$

where $\dot{S}_C$ is a source term that is used to inject the tracer into var ious zones in the domain, as described above. The diffusion coeffi cient D_f was set to give a Schmidt number of 1000. The concentration value was set to zero at the inlet and at the start of the simulation.

As will be evident in the next section, extremely fine meshes are needed to avoid numerical diffusion of the high Schmidt number scalars. Our previous simulations to study the hydrodynamics (Avila et al., 2020) used ANSYS CFX, simulating a wedge of the true geometry. However, for the study of mass transfer it soon became evident that massively finer meshes are needed and that there would be significant benefits in using ANSYS Fluent for these sim ulations. This is because ANSYS Fluent allows the use of a true 2D axisymmetric solver, thereby reducing the mesh requirement and reducing the number of equations to be solved. It also contains non iterative solvers that provide very fast transient simulations. Here the fractional timestep method was employed to couple pres sure and velocity. Finally, ANSYS Fluent has high order differencing schemes, which are not present in ANSYS CFX. Here gradients were calculated by the Green Gauss nodal scheme, pressure via a second order method, momentum using the third order QUICK scheme, mass fractions using the third order bounded MUSCL scheme and the bounded second order scheme was applied to the time deriva tives. A non dimensional local residual convergence target was set to 10 ^{5}.

3.2. Meshing and solution independence

Simulations were performed to determine the mesh require ment to obtain effectively mesh independent solutions. The 2D mesh was constructed in ANSYS Meshing using a paving algorithm, which used mostly quadrilateral cells whilst occasionally introduc ing triangular cells to fit geometric constraints. The starting point was a mesh size of 350 μm that was shown to give mesh indepen dent simulations for the hydrodynamics (Avila et al., 2020); this mesh was then progressively refined with the smallest cell size used being 30 μm.

Several cases with different oscillating and net flow operating conditions were studied, however for the sake of brevity, only the worst case scenario is presented. This occurs when there is high net flow causing high Péclet numbers. Fig. 3 contains the mesh dependency of the axial velocity and the tracer concentration when released from the axis and mid baffle sources. Data are pre sented in non dimensional form. It is evident from Fig. 3(a) that the velocity field is mesh independent using a 350 μm mesh, which is consistent with the observation made in our earlier work using ANSYS CFX (Avila et al., 2020). However, when using this mesh size, the concentrations are highly diffused. For the axial injection (Source 0) the results are almost mesh independent for a 100 μm mesh and are definitely independent for a 50 μm mesh. For Source 1 it is apparent that the very thin striation is not yet fully mesh independent for the 30 μm mesh but the shape of the profile is not too different to that for the 50 μm mesh.

Based on the above results and the analysis of other cases, it was decided to use a 50 μm mesh as a good compromise between accuracy and computing time. This mesh size gave a cell count of 1.46 million for the computational domain. Additionally, timestep independence was tested and observed to be achieved with 500 steps per period. The use of second order time differencing proved to be important in achieving independence with this timestep size.

4. Results and discussion

To study the effect of oscillatory conditions and tracer source position (as shown in Fig. 2(b)) on the mixing performance in the

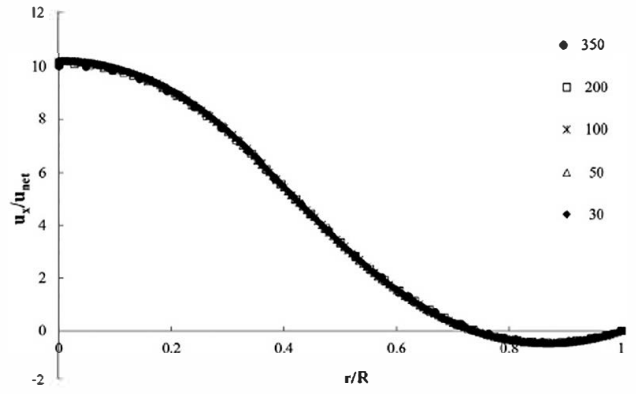

(a)

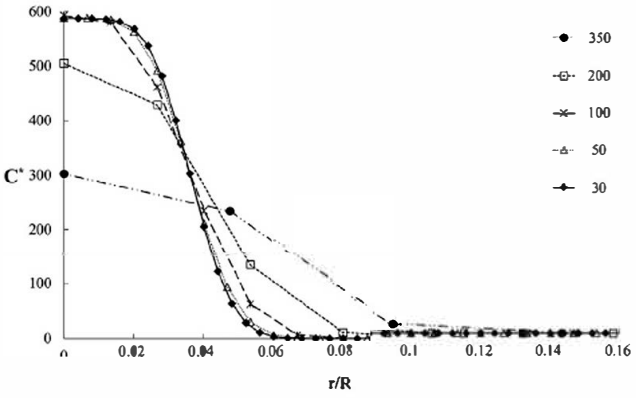

(b)

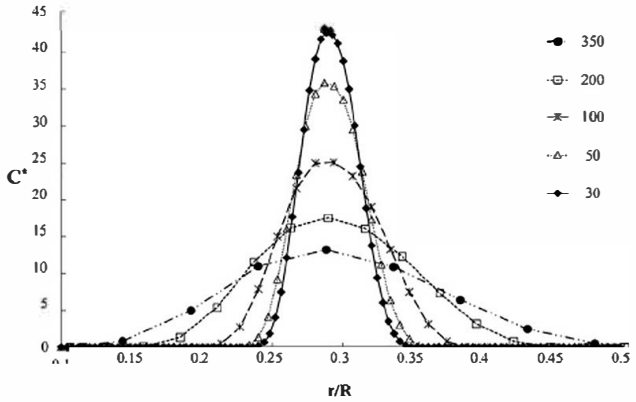

(c)

Fig. 3. Radial variation of (a) axial velocity and scalars released (b) at the axis (Source 0) and (c) mid-baffle (Source 1) at one quarter of the time through the first period for Case 1. The legend gives the mesh size in microns.

COBR, the dispersion of an inert tracer was simulated. Mixing performance was assessed after the average tracer concentration values at the different monitoring planes had reached a pseudo steady state (i.e. data do not present differences between consecutive oscillatory periods).

4.1. Flow and tracer patterns

Fig. 4 shows the velocity vectors over an oscillatory cycle for Case 5 (Re_{net} 6, Re_o 24, $\psi = 4$). In this figure, the process of flow separation, generation, propagation and detachment of vortices can be observed at different stages of flow acceleration and deceleration during the oscillatory period. During the start of acceleration (for both the forward and backward phases, Fig. 4(a) and (d)), flow separation begins and small eddy structures, which are not longer than the baffle width, are generated in front or behind the baffle constrictions, depending of the direction of the flow. As the cycle progresses, the toroidal vortex propagates towards the next baffle, until the flow speed reaches its maximum value (Fig. 4(b) and (e)). Once the flow reversal phase starts, the vortex grows to fill most of the space between the baffles until the flow begins to be completely reversed (Fig. 4(c) and (f)). With the decrease of the velocity during the flow reversal, the vortex acts as an obstacle. This makes the flow move along the reactor wall, detaching the toroidal vortex from the wall and engulfing it into the centre of the reactor at the start of flow acceleration and the cycle starts again (Fig. 4(a)). The generation and presence of vortices in the baffle area and their displacement from the wall to the centre of the reactor ensures radial mixing, unlike laminar flow in a straight tube. These flow patterns have already been identified in both OBR and COBR in the literature (Brunold et al., 1989; Gough et al., 1997; Mazubert et al., 2016a; Ni et al., 2002).

The tracer patterns are strongly influenced by the synergy of the source position, and the net and oscillatory flows. To better understand this interaction, Fig. 5 shows the evolution of the tracer distribution over one oscillatory cycle for the different source locations using Case 1 as an example. Case 1 has a net Reynolds number of 27 and a velocity ratio equal to 0.9. Fig. 5(a) shows that when the tracer is introduced at the centre of the tube, it is transported down the central axis of the reactor, creating a region of highly concentrated tracer. The eddies created by the interaction of the oscillatory flow with the baffles do not enable effective radial mixing of the tracer. On the other hand, when the tracer is introduced from Source 1, which is in line with the baffle edge midway between the centre and the wall of the tube as shown in Fig. 5(b), it can be seen that there is an improvement in radial mixing of the tracer along the reactor, resulting in an increase in the homogeneity and reaching values of C^* between 25 and 75% in the length of reactor simulated. A region of highly concentrated tracer is still present; however, it is disrupted by the baffle edge and then moves down the reactor over the oscillation cycle. This pattern allows shorter mixing lengths to be obtained compared with Source 0. Fig. 5(c) shows the concentration fields when the tracer is introduced at the wall at Source 2. In this case, the tracer moves slowly along the wall (where the axial velocity is close to zero), until it reaches the first orifice baffle. Due to the interaction of the oscillatory flow with the baffles and the subsequent eddies that are created, the tracer is then distributed radially. However, unlike with Source 1, a jet of fluid without tracer dominates the centreline of the reactor that is slowly mixed with the tracer by diffusion as the flow moves down the reactor.

4.2. Mixing performance

The mixing quality in the COBR can be quantified by analysing the tracer concentrations at different cross sections using the areal based distribution of mixing method. Fig. 6 gives an example of concentration fields on Plane 4 for Case 1 when the tracer is introduced at the wall (Source 2). This figure highlights the inhomogeneity of tracer concentration across the cross section. The data are used to determine distributions of mixing quality. Figs. 7 and 8 present the distributions of mixing quality (averaged over one oscillation period) at Plane 4 for the different cases studied and two different source positions, Source 1 and Source 2. These distributions enable the impact of operating conditions on mixing

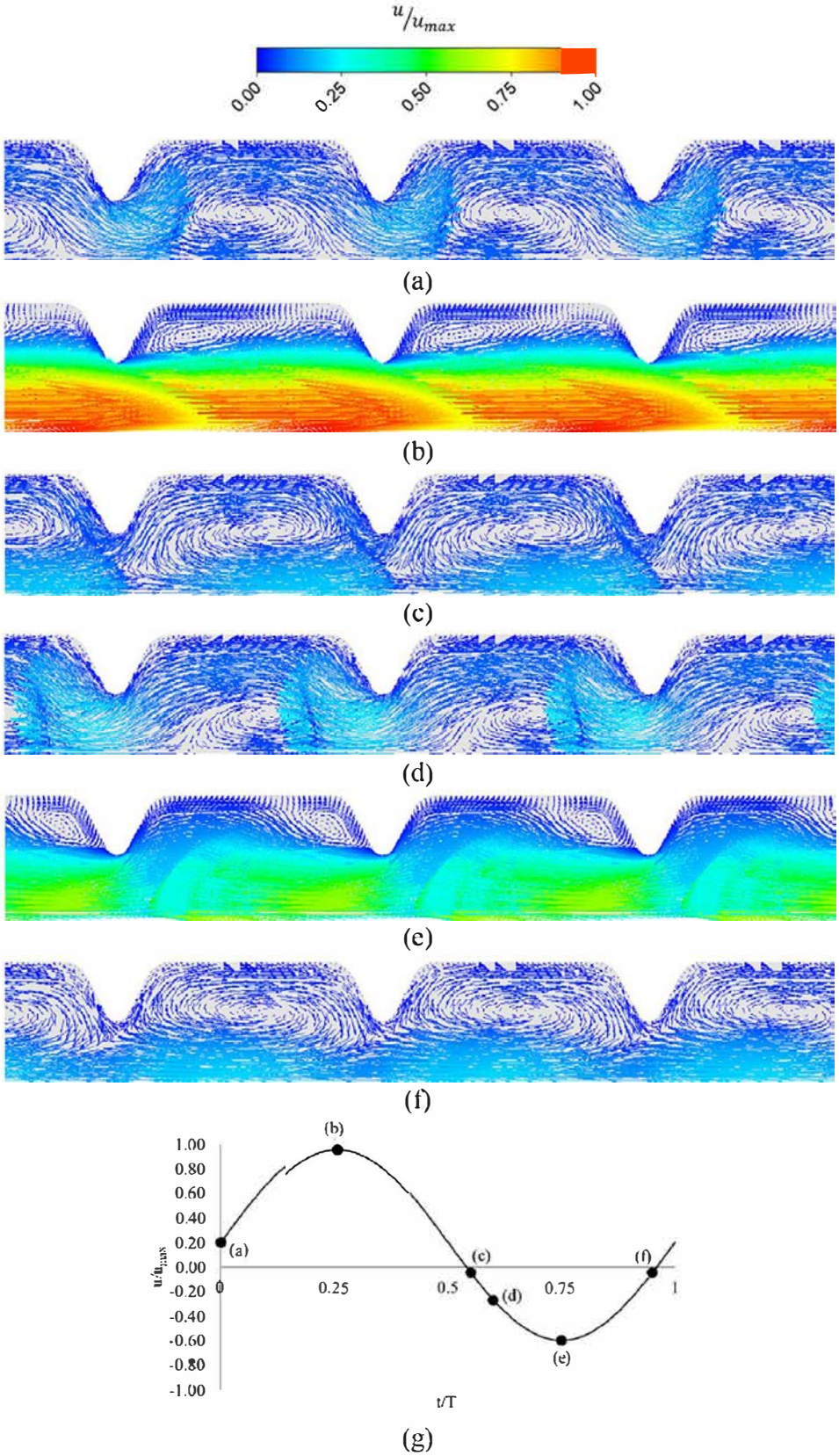

Fig. 4. Velocity vectors during the oscillatory flow for Case 5 (Re_{net} 6, f 1 Hz, x_o 5 mm): (a) t/T = 0.00, (b) t/T = 0.25, (c) t/T = 0.55, (d) t/T = 0.6, (e) t/T = 0.75, (f) t/T = 0.95, (g) normalized inlet velocity over an oscillatory period for Case 5 with the representation of the positions of the different times t/T during the period.

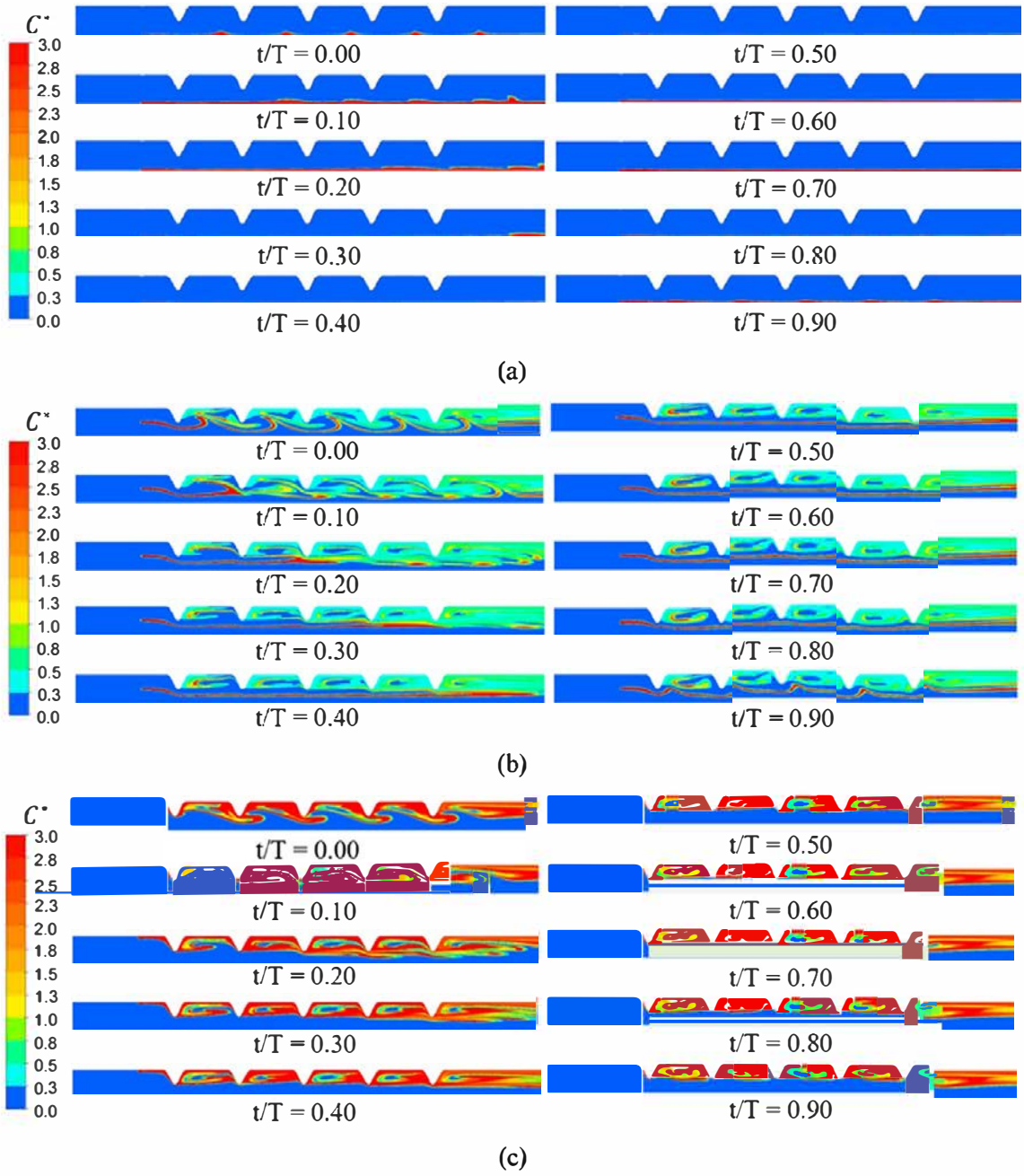

Fig. 5. Effect of source position on tracer patterns over a flow period(T) for Case 1 (Re_{net} 27, f 1 Hz, x_o 5 mm): (a) Source 0, (b) Source 1, (c) Source 2.

quality to be clearly seen and will be discussed in detail in the fol lowing paragraphs.

4.2.1. Influence of the frequency

The influence of the oscillatory frequency on the mixing perfor mance can be studied by comparing Cases 1 & 2, Cases 3 & 4, Cases 5 & 7 and Cases 6 & 8 in Figs. 7 and 8 for Source 1 and Source 2, respectively. For both source positions and for almost all cases, an increase in oscillation frequency (from 1 to 2 Hz) improves the mixing quality. An exception to this is at high oscillation ampli tude (x_o/l_b 0.6) and a low net Reynolds number (Re_{net} 6), i.e. Cases 6 and 8, whereby the increased oscillation frequency in Case 8 does not improve mixing performance. An explanation for this is discussed in Section 4.2.5.

4.2.2. Influence of the amplitude

The effect of the oscillation amplitude on mixing can be assessed by comparing Cases 1 & 3, Cases 2 & 4, Cases 5 & 6 and Cases 7 & 8. In all cases, the amplitude is increased from 5 to 10 mm at different net Reynolds numbers. An analysis of these results shows that there is no clear trend of the effect of oscillation amplitude on mixing quality, neither for high nor low net Reynolds numbers. This is different than what is observed for mixing in batch OBRs, whereby higher oscillatory conditions typically lead to improved mixing (Mackley and Neves Saraiva, 1999; Ni et al., 1998). Indeed, isolating the effect of oscillatory flow on mixing COBRs without taking into account the influence of the net flow is extremely complicated since it is the interaction between the pulsed flow, the net flow and the baffles that generates complex

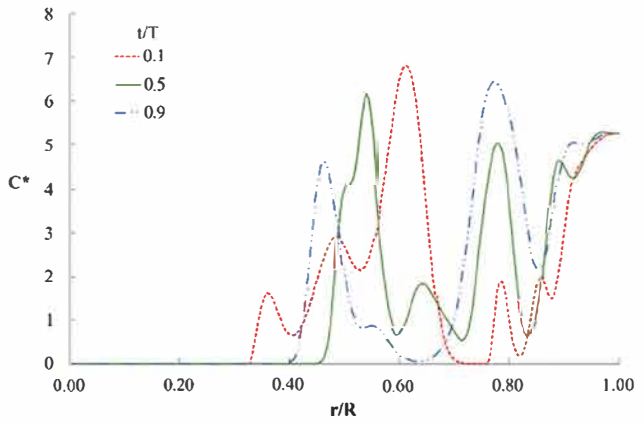

Fig. 6. Tracer profiles from Source 2 over a flow period (T) at Plane 4 for Case 1 (Re_{net} 27, f 1 Hz, x_o 5 mm).

flow patterns that are responsible for mixing (Mazubert et al., 2016a).

4.2.3. Synergy of the oscillatory frequency and amplitude

Comparison of Cases 2 & 3 (Re_{net} 27, Re_o 48, ψ = 1.8) and Cases 6 & 7 (Re_{net} 6, Re_o 48, ψ = 8) enables the impact of oscillatory conditions and net Reynolds number on mixing to be assessed. At the same oscillatory Reynolds number and velocity ratio, working with high frequencies and small amplitudes results in better mixing quality than with low frequencies and high amplitudes. For cases with ψ = 1.8 (Cases 2 & 3) and ψ = 8 (Cases 6 & 7) and Source 1, the interaction of the tracer with the baffle due to the pulsed flow is similar to that shown in Fig. 5(b) for Case 1. However, at higher amplitudes the tracer is transported further with each oscillation and it does not have the possibility to mix sufficiently in short distances. On the other hand, a smaller amplitude allows better interaction of the tracer with the flow and faster mixing. Cases with ψ = 8 demonstrate better mixing quality than cases with ψ = 1.8 due to the higher velocity ratio. Indeed, the lower net flow rate allows the tracer to spend more time in the cell between two baffles, where it is recirculated and mixed due to the generated eddies before being transported along the reactor to the next cell.

4.2.4. Influence of the source position

Fig. 9 presents a summary of the mixing quality at different axial positions along the COBR for all of the different operating conditions and tracer source positions. The graph shows the area fraction of each plane that is well mixed, i.e. that corresponds to >90% of the perfectly mixed state. The effect of the source position can be clearly observed by comparing Fig. 9(a), (b) and (c). In a general manner, as is expected, all source positions show that mixing performance improves along the reactor. Source 2 from Case 8 is an exception to this and is discussed later. When the tracer is introduced at the centre of the tube (Source 0), poor mixing performance is observed for most operating conditions since the tracer is transported down the centreline of the reactor without interacting with the recirculating eddies. This source position results in significant axial dispersion and radial mixing is limited, reaching values up to 30% of the perfectly mixed state in the best cases. There is a clear improvement in mixing quality when the tracer source is close to the reactor wall (Source 2). It is interesting to point out that this is a different result than that found by Alberini et al. (2014b) for mixing in a Kenics static mixer. They found poorest mixing performance with a wall source, whilst the central source provided good mixing. Indeed, a static mixer element spans the entire cross section of the tube so high axial dispersion along the centreline of the tube is not possible, unlike in the single orifice baffle geometry studied here. It is expected that mixing would be greatly improved in the COBR with a centreline source if other baffle geometries, e.g. multiple orifice plates or even static mixer elements, are used.

4.2.5. Influence of the velocity ratio

In a general manner, it can be seen from Fig. 9 that the net Reynolds number also plays an important role in mixing. In laminar flow, a lower net Reynolds number provides improved mixing quality and shorter mixing lengths since the residence time is longer and the tracer has more time to recirculate and mix by diffusion. However, the ratio of the oscillatory flow to the net flow, or velocity ratio, is also important and the impact of this is shown by comparing Cases 1 & 5, Cases 3 & 6, Cases 4 & 8, and Cases 2 & 7, in which case the oscillatory conditions are kept constant and the velocity ratio is increased by decreasing the net Reynolds number. In general, an increase in the velocity ratio results in an improved mixing performance. To understand this better, the tracer concentration fields for Case 7 (ψ = 8) and all three source locations are shown in Fig. 10. When operating with a higher velocity ratio, i.e. the oscillatory flow dominates, the net flow does not transport the tracer too far along the reactor, allowing it to mix and diffuse in the cells between baffles due to the recirculating flow. Nevertheless, it appears that if the velocity ratio is too high, mixing performance is hindered and this is illustrated with the results of Case 8, where ψ = 16, as shown in Fig. 11. Under this condition, the net flow has a small influence on the oscillatory flow and the COBR starts to operate more like a batch OBR. In this case, a large portion of the tracer gets pushed backwards, upstream of the source position, such that the tracer starts to mix before reaching the baffled zone. However, mixing here is slow since there are no recirculating eddies to enhance the transport process. Mixing quality would be expected to improve for the same operating conditions if the source location is situated within the baffled zone. In this position, the dye that is pushed upstream will still be within the baffle zone, profiting from eddies and recirculation flow (similar to those for Case 7), and enhancing mixing performance. When the tracer source is close to the wall where the axial velocity is close to zero, the tracer spends more time in the vicinity of the source before being pushed down the reactor, explaining the better mixing performance at early planes seen in Fig. 9(c).

The velocity ratio has an important influence in the reversed flow phase of the oscillatory cycle. When ψ = 0.9 (Case 1), the net flow dominates over the oscillatory flow, causing the reverse flow portion of the cycle to be small. The absence of fully reversing flow causes a deceleration of the net flow. This condition does not allow the eddies created between consecutive baffles to move to the centre of the reactor due to the difference between the velocity magnitudes at the centreline and the baffle zone, which increases axial mixing and decreases radial mixing. As ψ increases, the time fraction over which reverse flow occurs during the oscillatory cycle increases and the vortices start to interact with the net flow, enhancing radial mixing and decreasing axial mixing. For ψ = 1.8 (Cases 2 & 3) reverse flow occurs for $\Delta t/T$ 0.3 of the overall flow cycle, at ψ = 8 (Cases 6 & 7) it is for $\Delta t/T$ 0.46 and at ψ = 16 (Case 8) it is for $\Delta t/T$ 0.48. As ψ increases, the COBR behaves more like a batch OBR, having reverse flow at close to $\Delta t/T$ 0.5. For some value of the velocity ratio between ψ = 8 and ψ = 16, the influence of the reverse flow over the net flow becomes preponderant and the oscillatory conditions become detrimental to the mixing performance due the backward flux of tracer. This explains the reduction of mixing performance when increasing the frequency from 1 Hz in Case 6, to 2 Hz in Case 8.

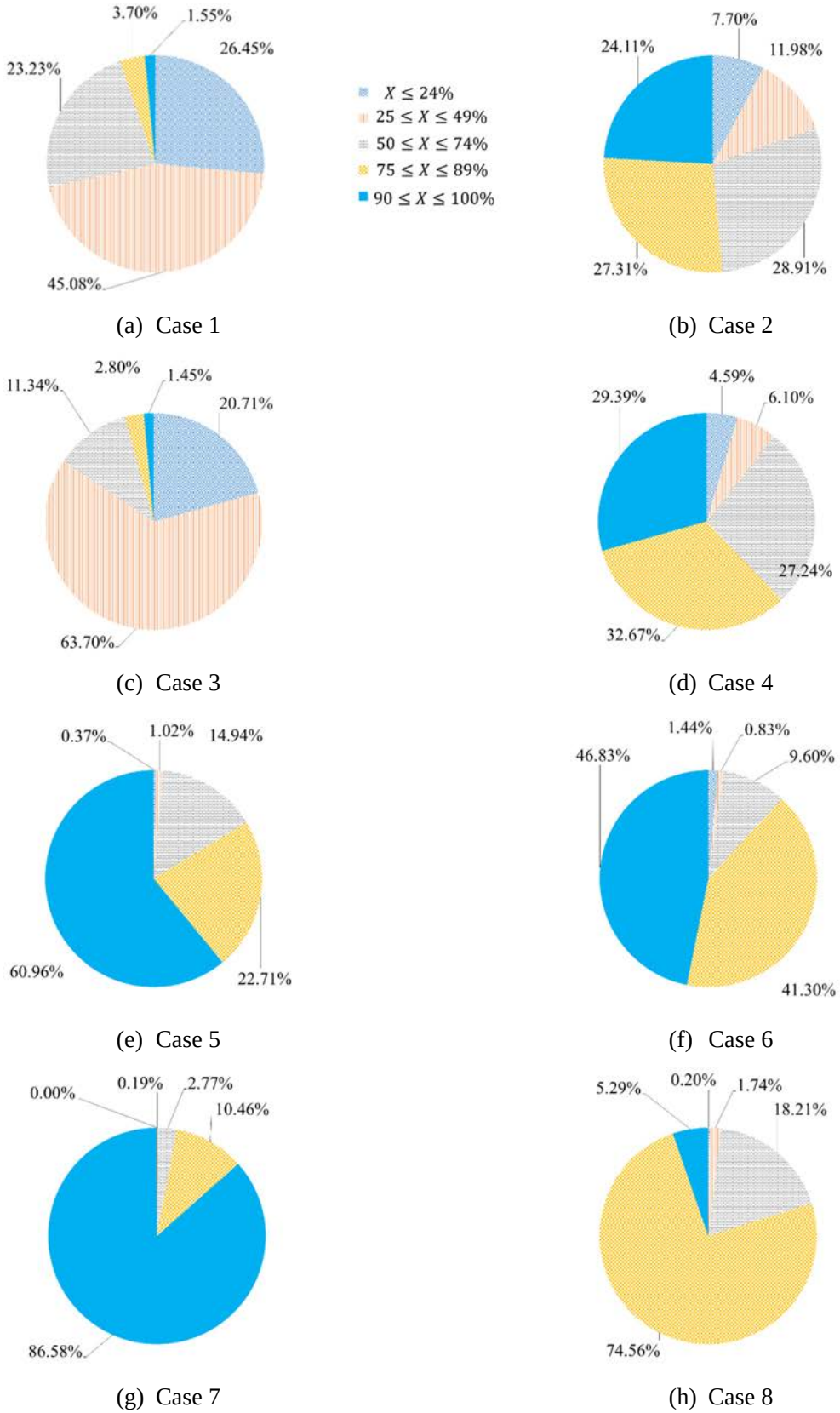

Fig. 7. Areal distribution of mixing intensity averaged over one oscillation period at Plane 4 for Source 1: (a) Case 1, (b) Case 2, (c) Case 3, (d) Case 4, (e) Case 5, (f) Case 6, (g) Case 7, (h) Case 8.

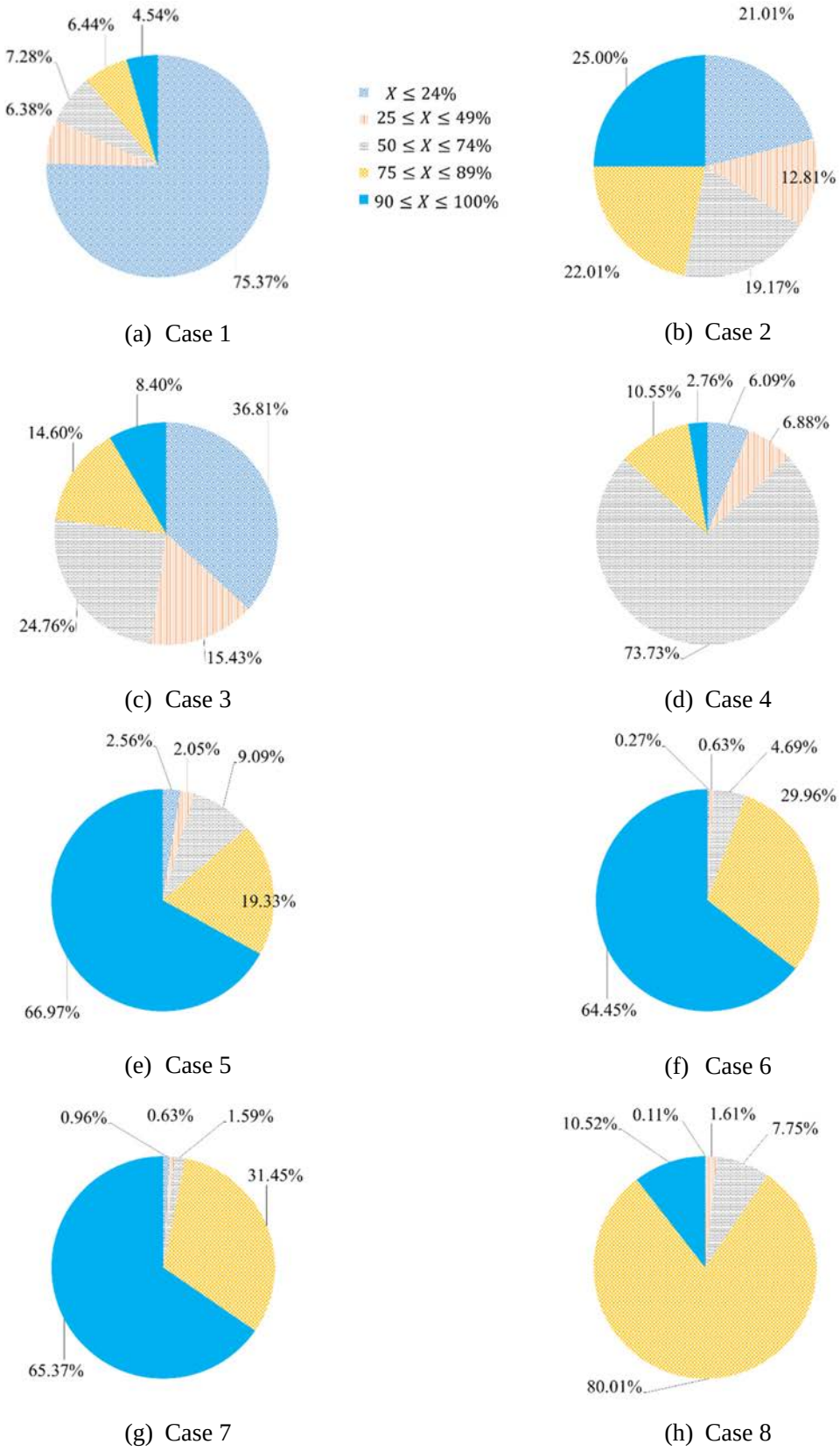

Fig. 8. Areal distribution of mixing intensity averaged over one oscillation period at Plane 4 for Source 2: (a) Case 1, (b) Case 2, (c) Case 3, (d) Case 4, (e) Case 5, (f) Case 6, (g) Case 7, (h) Case 8.

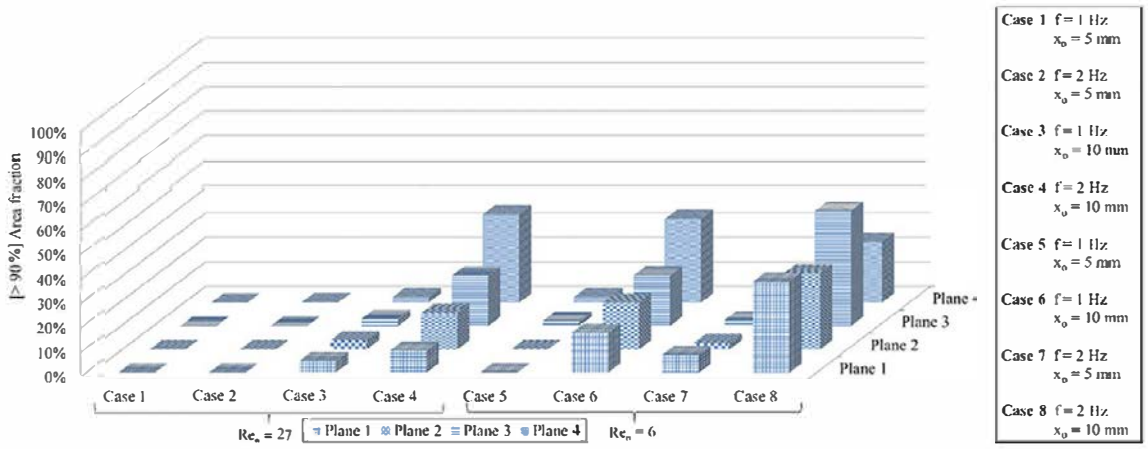

(a)

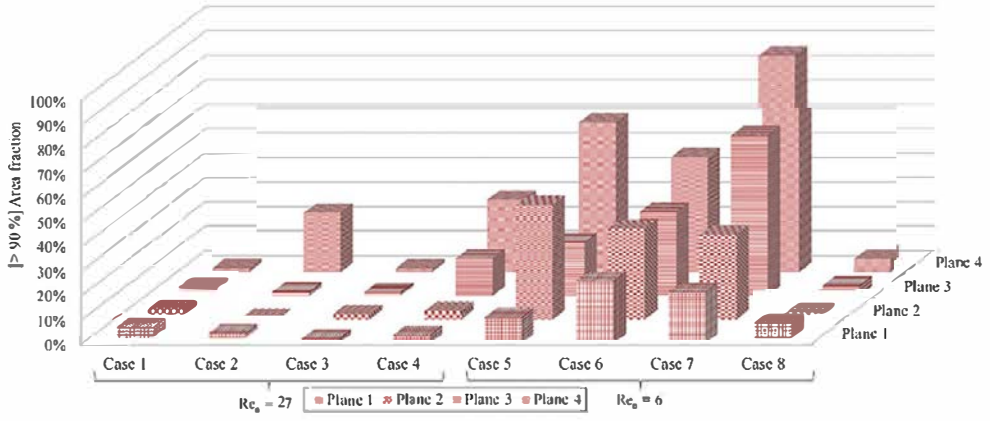

(b)

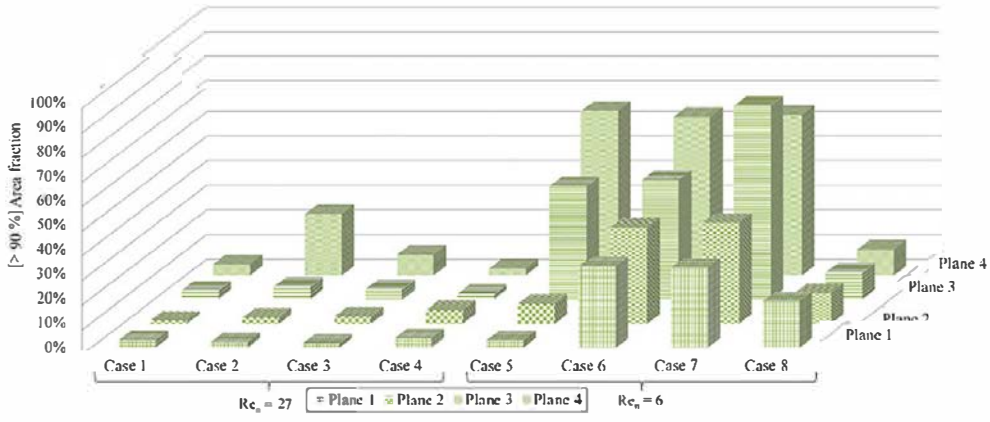

(c)

Fig. 9. Area fraction of Planes 1, 2, 3, and 4 (averaged over one oscillation period) where >90% mixing is achieved for Cases 1 to 8. (a) Source 0; (b) Source 1; (c) Source 2.

5. Conclusions

The impact of oscillatory and flow parameters (frequency, amplitude and velocity ratio) and tracer source position on mixing quality in a COBR were studied through CFD simulations. Introduction of the tracer at the reactor wall or approximately midway between the wall and the centre of the tube (in front of the first orifice baffle) results in significantly better mixing performance than when it is introduced at the tube centreline. The latter results in high axial dispersion with limited radial mixing; this is primarily due to the orifice baffle geometry. Introduction of the tracer away from the tube centreline enables improved radial mixing due to the recirculation eddies created by the interaction of the baffles and the pulsed flow. A simple change in the source position can increase this to values of 87% of the perfectly mixed state (where >90% of mixing is achieved).

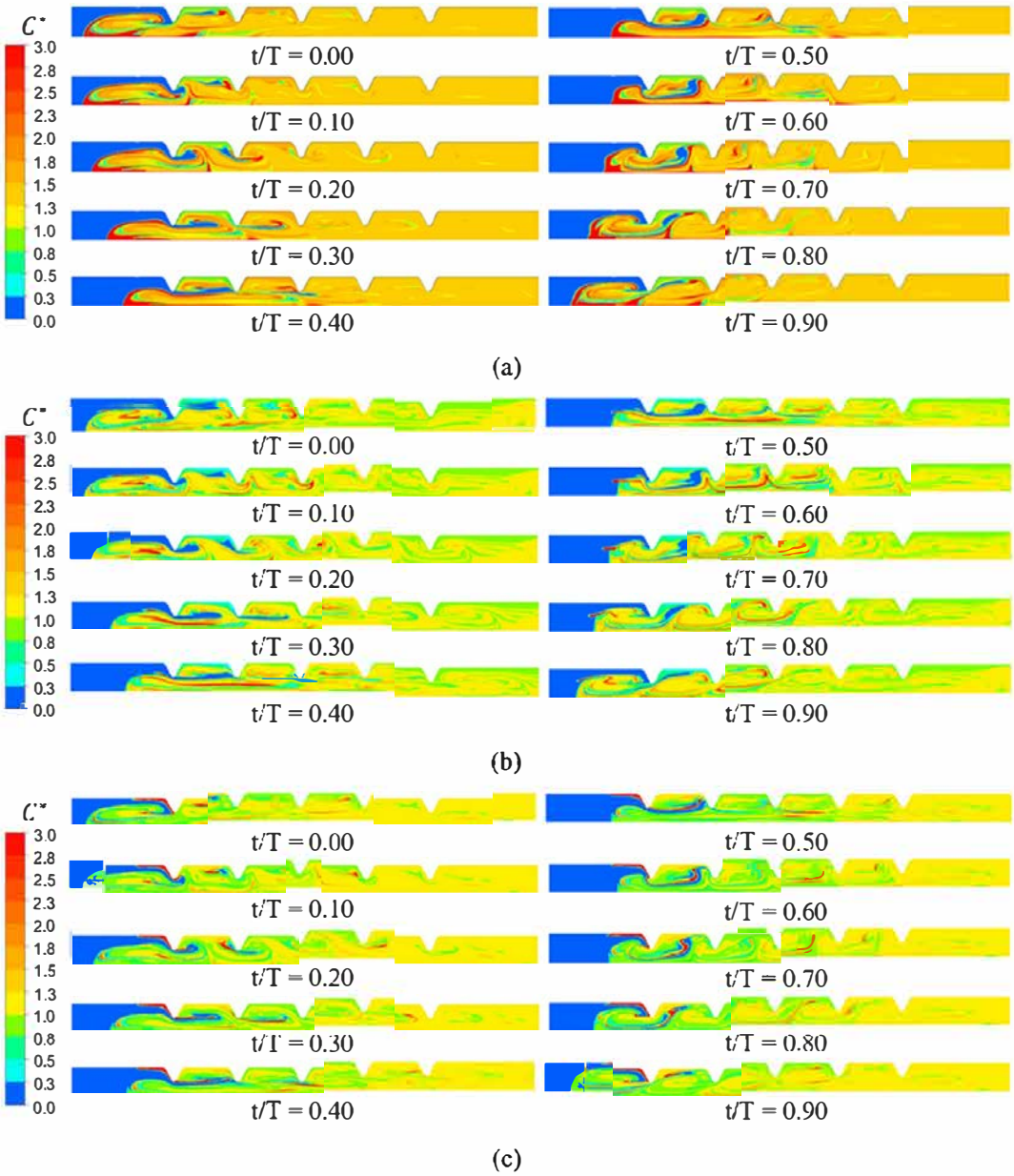

Fig. 10. Tracer patterns over a flow period(T) for Case 7 (Re_{net} 6, f 2 Hz, x_o 5 mm): (a) Source 0, (b) Source 1, (c) Source 2.

An increase in the frequency usually leads to an improvement in mixing quality, contrary to an increase in the amplitude, where no clear trend was found. The interaction between the oscillatory flow, the net flow and the baffles make it difficult to characterise mixing by taking into account only the oscillatory conditions (i.e. f and x_o). For a fixed oscillatory Reynolds number, higher oscillation frequencies with amplitudes close to $0.3l_b$ (which is close to the value recommended by Gough et al. 1997, i.e. 25% of baffle spacing from a simple experimental observation of flow patterns in a pulsed baffled reactor) provide better mixing than low frequencies and high amplitudes. Mixing quality typically increases with an increase in the velocity ratio, provided that an adequate position of the source is chosen, enabling the tracer to be convected by the recirculation eddies created by the interac tion of the pulsed flow with the baffles. The increase of velocity ratio enhances mixing quality from poorly mixed conditions (less than 4% of the perfect mixed state) up to 87% of the perfectly mix ing state. From previous studies, the recommended velocity ratio to obtain plug flow in a COBR is ψ 2 4 (Stonestreet and Van Der Veeken, 1999). However, this work shows that higher velocity ratios are preferred to obtain uniform spatial mixing rapidly, which highlights that different operating conditions may be required depending on the process objective (Kacker et al., 2017; Soufi et al., 2017). The magnitude of the net flow is also important. If the net flow is too low, mixing may be hindered because the secondary stream (tracer) is pushed upstream of the baffles, where it does not benefit from flow recirculation. In such a case, it is expected that introduction of the secondary stream in the baffled region, rather than upstream, would greatly improve mixing. These results provide a first estimate of where the plume of an injection jet needs to be positioned for future studies.

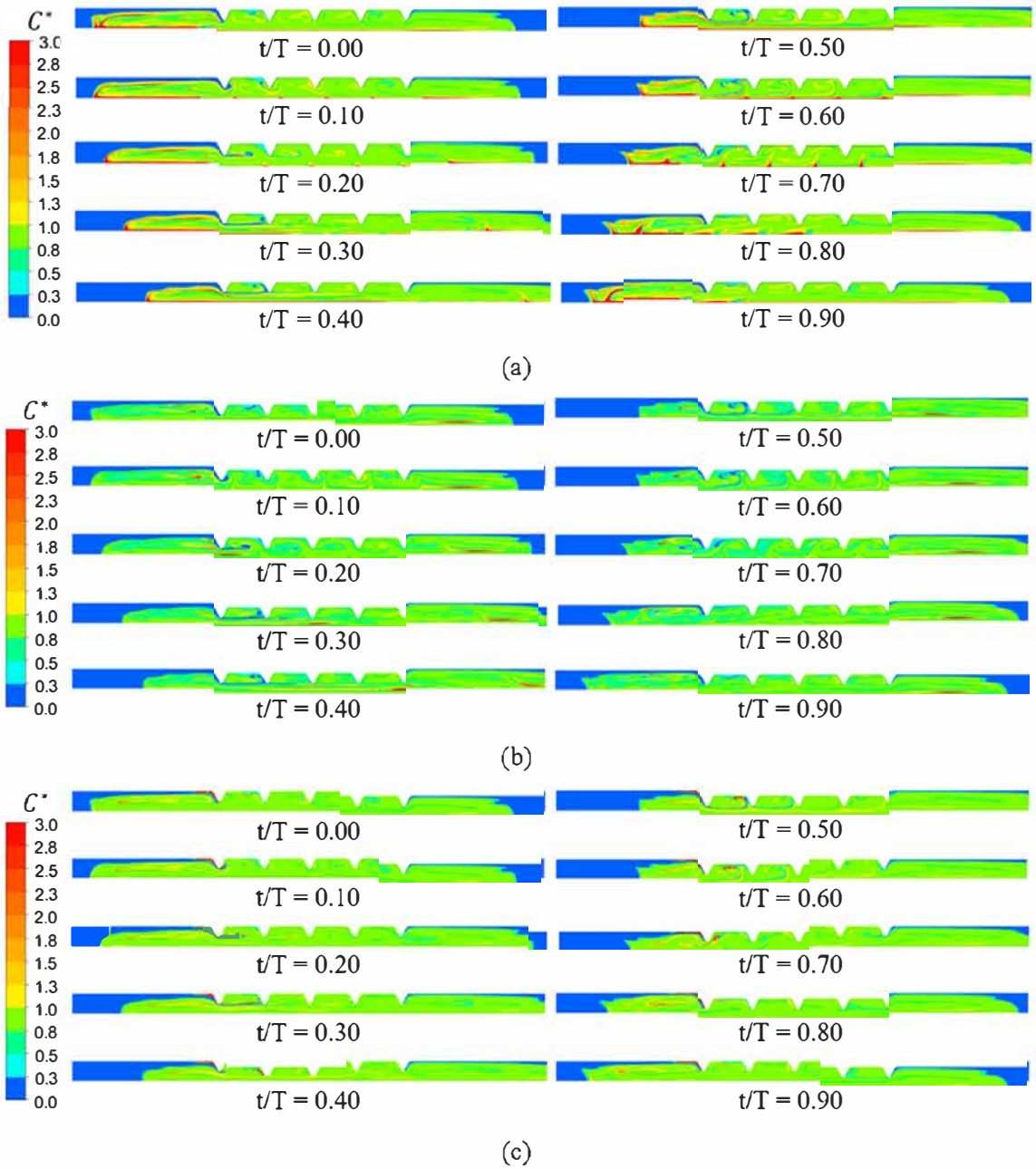

Fig. 11. Tracer patterns over a flow period(T) for Case 8 (Re_{net} 6, f 2 Hz, x_o 10 mm): (a) Source 0, (b) Source 1, (c) Source 2.

CRediT authorship contribution statement

M. Avila: Conceptualization, Formal analysis, Investigation, Writing original draft. **D.F. Fletcher:** Methodology, Software, Writing review & editing, Supervision. **M. Poux:** Supervision. **C. Xuereb:** Supervision. **J. Aubin:** Conceptualization, Writing review & editing, Supervision.

Declaration of Competing Interest

The authors declare that they have no known competing financial interests or personal relationships that could have appeared to influence the work reported in this paper.

Acknowledgements

The authors acknowledge the University of Sydney's high performance computing cluster Artemis for providing High Performance Computing resources that have contributed to the research results reported in this paper, as well as the Mexican Council of Science and Technology (CONACYT México) and Toulouse INP for diverse funding.

References

Abbott, M.S.R., Harvey, A.P., Morrison, M.I., 2014. Rapid determination of the Residence time distribution (RTD) function in an oscillatory baffled reactor (OBR) using a design of experiments (DoE) approach. Int. J. Chem. React. Eng. 12, 575–586. https://doi.org/10.1515/ijcre-2014-0040.

Abbott, M.S.R., Harvey, A.P., Valente Perez, G., Theodorou, M.K., 2013. Biological processing in oscillatory baffled reactors: Operation, advantages and potential. Interface Focus 3, 20120036. https://doi.org/10.1098/rsfs.2012.0036.

Ahmed, S.M.R., Phan, A.N., Harvey, A.P., 2017. Scale-up of oscillatory helical baffled reactors based on residence time distribution. Chem. Eng. Technol. 40, 907–914. https://doi.org/10.1002/ceat.201600480.

Alberini, F., Simmons, M.J.H., Ingram, A., Stitt, E.H., 2014a. Use of an areal distribution of mixing intensity to describe blending of non-newtonian fluids in a Kenics KM static mixer using PLIF. AIChE J. 60, 332–342. https://doi.org/10.1016/j.ces.2014.03.022.

Alberini, F., Simmons, M.J.H., Ingram, A., Stitt, E.H., 2014b. Assessment of different methods of analysis to characterise the mixing of shear-thinning fluids in a Kenics KM static mixer using PLIF. Chem. Eng. Sci. 112, 152–169. https://doi.org/10.1016/j.ces.2014.03.022.

Amokrane, A., Charton, S., Lamadie, F., Paisant, J.F., Puel, F., 2014. Single-phase flow in a pulsed column: particle image velocimetry validation of a CFD based model. Chem. Eng. Sci. 114, 40–50. https://doi.org/10.1016/j.ces.2014.04.003.

Avila, M., Fletcher, D.F., Poux, M., Xuereb, C., Aubin, J., 2020. Predicting power consumption in continuous oscillatory baffled reactors. Chem. Eng. Sci. 212. https://doi.org/10.1016/j.ces.2019.115310.

Briggs, N.E.B.B., Schacht, U., Raval, V., McGlone, T., Sefcik, J., Florence, A.J., 2015. Seeded crystallization of β- L -glutamic acid in a continuous oscillatory baffled crystallizer. Org. Process Res. Dev. 19, 1903–1911. https://doi.org/10.1021/acs.oprd.5b00206.

Brunold, C.R.R., Hunns, J.C.B.C.B., Mackley, M.R.R., Thompson, J.W.W., 1989. Experimental observations on flow patterns and energy losses for oscillatory flow in ducts containing sharp edges. Chem. Eng. Sci. 44, 1227–1244. https://doi.org/10.1016/0009-2509(89)87022-8.

Dickens, A.W., Mackley, M.R., Williams, H.R., 1989. Experimental residence time distribution measurements for unsteady flow in baffled tubes. Chem. Eng. Sci. 44, 1471–1479. https://doi.org/10.1016/0009-2509(89)80023-5.

Eze, V.C., Fisher, J.C., Phan, A.N., Harvey, A.P., 2017. Intensification of carboxylic acid esterification using a solid catalyst in a mesoscale oscillatory baffled reactor platform. Chem. Eng. J. 322, 205–214. https://doi.org/10.1016/j.cej.2017.04.038.

González-Juárez, D., Solano, J.P., Herrero-Martín, R., Harvey, A.P., 2017. Residence time distribution in multiorifice baffled tubes: A numerical study. Chem. Eng. Res. Des. 118, 259–269. https://doi.org/10.1016/j.cherd.2016.12.008.

Gough, P., Ni, X., Symes, K.C., 1997. Experimental flow visualisation in a modified pulsed baffled reactor. J. Chem. Technol. Biotechnol. 69, 321–328. https://doi.org/10.1002/(SICI)1097-4660(199707)69.

Harvey, A.P., Mackley, M.R., Seliger, T., 2003. Process intensification of biodiesel production using a continuous oscillatory flow reactor. J. Chem. Technol. Biotechnol. 78, 338–341. https://doi.org/10.1002/jctb.782.

Harvey, A.P., Mackley, M.R., Stonestreet, P., 2001. Operation and optimization of an oscillatory flow continuous reactor. Ind. Eng. Chem. Res. 40, 5371–5377. https://doi.org/10.1021/ie0011223.

Hewgill, M.R., Mackley, M.R., Pandit, A.B., Pannu, S.S., 1993. Enhancement of gas-liquid mass transfer using oscillatory flow in a baffled tube. Chem. Eng. Sci. 48, 799–809. https://doi.org/10.1016/0009-2509(93)80145-G.

Kacker, R., Regensburg, S.I., Kramer, H.J.M.M., 2017. Residence time distribution of dispersed liquid and solid phase in a continuous oscillatory flow baffled crystallizer. Chem. Eng. J. 317, 413–423. https://doi.org/10.1016/j.cej.2017.02.007.

Kukukova, A., Aubin, J., Kresta, S.M., 2011. Measuring the scale of segregation in mixing data. Can. J. Chem. Eng. 89, 1122–1138. https://doi.org/10.1002/cjce.20532.

Kukukova, A., Aubin, J., Kresta, S.M., 2009. A new definition of mixing and segregation: three dimensions of a key process variable. Chem. Eng. Res. Des. 87, 633–647. https://doi.org/10.1016/j.cherd.2009.01.001.

Lobry, E., Lasuye, T., Gourdon, C., Xuereb, C., 2014. Liquid-liquid dispersion in a continuous oscillatory baffled reactor - application to suspension polymerization. Chem. Eng. J. 259, 505–518. https://doi.org/10.1016/j.cej.2014.08.014.

Mackley, M.R., Neves Saraiva, R.M.C., 1999. The quantitative description of fluid mixing using Lagrangian- and concentration-based numerical approaches. Chem. Eng. Sci. 54, 159–170. https://doi.org/10.1016/S0009-2509(98)00169-9.

Mackley, M.R., Ni, X., 1993. Experimental fluid dispersion measurements in periodic baffled tube arrays. Chem. Eng. Sci. 48, 3293–3305. https://doi.org/10.1016/0009-2509(93)80213-A.

Mackley, M.R., Ni, X., 1991. Mixing and dispersion in a baffled tube for steady laminar and pulsatile flow. Chem. Eng. Sci. 46, 3139–3151. https://doi.org/10.1016/0009-2509(91)85017-R.

Mackley, M.R., Stonestreet, P., 1995. Heat transfer and associated energy dissipation for oscillatory flow in baffled tubes. Chem. Eng. Sci. 50, 2211–2224.

Manninen, M., Gorshkova, E., Immonen, K., Ni, X.W., 2013. Evaluation of axial dispersion and mixing performance in oscillatory baffled reactors using CFD. J. Chem. Technol. Biotechnol. 88, 553–562. https://doi.org/10.1002/jctb.3979.

Mazubert, A., Crockatt, M., Poux, M., Aubin, J., Roelands, M., 2015. Reactor comparison for the esterification of fatty acids from waste cooking oil. Chem. Eng. Technol. 38, 2161–2169. https://doi.org/10.1002/ceat.201500138.

Mazubert, A., Fletcher, D.F., Poux, M., Aubin, J., 2016a. Hydrodynamics and mixing in continuous oscillatory flow reactors—Part I: Effect of baffle geometry. Chem. Eng. Process. Process Intensif. 108, 78–92.

Mazubert, A., Fletcher, D.F., Poux, M., Aubin, J., 2016b. Hydrodynamics and mixing in continuous oscillatory flow reactors—Part II: Characterisation methods. Chem. Eng. Process. Process Intensif. 102, 102–116.

McDonough, J.R., Ahmed, S.M.R., Phan, A.N., Harvey, A.P., 2017. A study of the flow structures generated by oscillating flows in a helical baffled tube. Chem. Eng. Sci. J. 171, 160–178. https://doi.org/10.1016/j.ces.2017.05.032.

McDonough, J.R., Oates, M.F., Law, R., Harvey, A.P., 2019. Micromixing in oscillatory baffled flows. Chem. Eng. J. 361, 508–518. https://doi.org/10.1016/j.cej.2018.12.088.

Ni, X., 1995. A study of fluid dispersion in oscillatory flow through a baffled tube. J. Chem. Technol. Biotechnol. 64, 165–174. https://doi.org/10.1002/jctb.280640209.

Ni, X., Brogan, G., Struthers, A., Bennett, D.C., Wilson, S.F., 1998. A systematic study of the effect of geometrical parameters on mixing time in oscillatory baffled columns. Chem. Eng. Res. Des. 76, 635–642. https://doi.org/10.1205/026387698525162.

Ni, X., Cosgrove, J.A., Arnott, A.D., Greated, C.A., Cumming, R.H., 2000. On the measurement of strain rate in an oscillatory baffled column using particle image velocimetry. Chem. Eng. Sci. 55, 3195–3208. https://doi.org/10.1016/S0009-2509(99)00577-1.

Ni, X., Jian, H., Fitch, A., 2003. Evaluation of turbulent integral length scale in an oscillatory baffled column using large eddy simulation and digital particle image velocimetry. Chem. Eng. Res. Des. 81, 842–853. https://doi.org/10.1205/026387603322482086.

Ni, X., Jian, H., Fitch, A.W., 2002. Computational fluid dynamic modelling of flow patterns in an oscillatory baffled column. Chem. Eng. Sci. 57, 2849–2862. https://doi.org/10.1016/S0009-2509(02)00081-7.

Peña, R., Oliva, J.A., Burcham, C.L., Jarmer, D.J., Nagy, Z.K., 2017. Process intensification through continuous spherical crystallization using an oscillatory flow baffled crystallizer. Cryst. Growth Des. 17, 4776–4784. https://doi.org/10.1021/acs.cgd.7b00731.

Phan, A.N., Harvey, A., 2010. Development and evaluation of novel designs of continuous mesoscale oscillatory baffled reactors. Chem. Eng. J. 159, 212–219. https://doi.org/10.1016/j.cej.2010.02.059.

Phan, A.N., Harvey, A.P., 2011. Characterisation of mesoscale oscillatory helical baffled reactor - experimental approach. Chem. Eng. J. 180, 229–236. https://doi.org/10.1016/j.cej.2011.11.018.

Phan, A.N., Harvey, A.P., Eze, V., 2012. Rapid production of biodiesel in mesoscale oscillatory baffled reactors. Chem. Eng. Technol. 35, 1214–1220. https://doi.org/10.1002/ceat.201200031.

Reis, N., Vicente, A.A., Teixeira, J.A., Mackley, M.R., 2004. Residence times and mixing of a novel continuous oscillatory flow screening reactor. Chem. Eng. Sci. 59, 4967–4974. https://doi.org/10.1016/j.ces.2004.09.013.

Siddique, H., Brown, C.J., Houson, I., Florence, A.J., 2015. Establishment of a continuous sonocrystallization process for lactose in an oscillatory baffled crystallizer. Org. Process Res. Dev. 19, 1871–1881. https://doi.org/10.1021/acs.oprd.5b00127.

Soufi, M.D., Ghobadian, B., Najafi, G., Mohammad Mousavi, S., Aubin, J., 2017. Optimization of methyl ester production from waste cooking oil in a batch tri-orifice oscillatory baffled reactor. Fuel Process. Technol. 167, 641–647. https://doi.org/10.1016/j.fuproc.2017.07.030.

Stephens, G., Mackley, M., 2002. Heat transfer performance for batch oscillatory flow mixing. Exp. Therm. Fluid Sci. 25, 583–594. https://doi.org/10.1016/S0894-1777(01)00098-X.

Stonestreet, P., Van Der Veeken, P.M.J., 1999. The effects of oscillatory flow and bulk flow components on residence time distribution in baffled tube reactors. Chem. Eng. Res. Des. 77, 671–684. https://doi.org/10.1205/026387699526809.

Zhao, L., Raval, V., Briggs, N.E.B., Bhardwaj, R.M., McGlone, T., Oswald, I.D.H., Florence, A.J., 2014. From discovery to scale-up: α-lipoic acid: nicotinamide co-crystals in a continuous oscillatory baffled crystalliser. CrystEngComm 16, 5769–5780. https://doi.org/10.1039/c4ce00154k.

Zheng, M., Li, J., Mackley, M.R., Tao, J., Zhengjie, M., Tao, L.R.M., Zheng, M., Li, J., Mackley, M.R., Tao, J., 2007. The development of asymmetry for oscillatory flow within a tube containing sharp edge periodic baffles. Cit. Phys. Fluids 19. https://doi.org/10.1063/1.2799553.